

Trajectory Tracking for Swing Phase of the Lower Limb Exoskeleton

Xiao Guan, Chun-Hao Zhong, Jie Huang and Wei-Hsin Liao

*Department of Mechanical and Automation Engineering
 The Chinese University of Hong Kong*

Shatin, Hong Kong, China

whliao@cuhk.edu.hk

Abstract - In this paper, the dynamic model of swing phase of the lower limb exoskeleton is firstly established. Based on the proposed model, system identification experiments at each joint are conducted to determine unknown parameters and joint friction torques by tracking desired reference signals. The experimental data are processed by the least squares method. Another validation experiment is taken to verify the accuracy of the estimated model. Both linear and nonlinear controllers are designed. The linear controller is a proportional-derivative (PD) controller, and the nonlinear controller is a PD controller with gravity and friction torque compensation. Experiments show that the transient response of the tracking performance of the nonlinear controller is significantly better than that of the linear controller.

Keywords - lower limb exoskeleton; trajectory tracking; system identification; gravity and friction compensation

I. INTRODUCTION

The lower limb exoskeletons (LLEs) are one type of wearable bionic devices, which are equipped with actuators at human lower limb [1]. According to different application purposes, the LLEs can mainly be classified as: (1) LLEs for gait assistance, such as Lokomat [2] and ALEX [3], (2) LLEs for locomotion assistance, such as ReWalk [4] and the Vanderbilt exoskeleton [5], (3) LLEs for human strength augmentation, such as BLEEX [6] and HAL [7].

The CUHK-Exoskeleton (CUHK-EXO) was developed for the paralyzed individuals since 2015, and it belongs to the categories of LLEs for locomotion assistance. The CUHK-EXO has totally six degrees of freedom (DOFs) and four of them (hip joint and knee joint) are active joints, which are regulated by DC motors [8]. The first prototype had three functions (sit down-stand up, stand up-sit down and ground walk), and the second prototype extended to go up/down stairs function. Since the sit down-stand up and stand up-sit down functions share the same dynamical model, two legs have symmetrical motions and the foot parts always have full contact with the ground, they can be considered as one motion (STS motion). The assistance strategies for STS motion was studied by Chen et al. by trajectory online modification method [9].

However, ground walk and go up/down stairs functions have asymmetrical trajectories for different legs, and the gait cycles of those functions can be further divided into swing phase and stance phase. During the stance phase, the foot part of support leg has contact with the ground, and the exoskeleton needs to provide sufficient torques to support its user. For the

swing phase, the swing leg is suspended by hip and knee joint actuators, and the tracking accuracy during the gait cycle plays an important role. If the swing leg cannot track desired trajectories precisely, the toe of foot part will hit the ground and the user of exoskeleton needs to make more efforts to keep balance. Therefore, control strategies for different phases are quite different, and this paper presents one solution to the swing phase control problem.

The original tracking strategy for the CUHK-EXO is pure PD controller, and the tracking error during the swing phase is around 10 degrees [1]. Castro et al. applied the linear quadratic regulator method to the second prototype of the CUHK-EXO, which can reduce tracking errors to be less than 5 degrees [10]. By Castro's method, one gait cycle is separated into 100 points, and control gains at each point are computed offline. According to the continuous walking test, the initial conditions for continuous gait cycles are quite different. Since online computing control gains with previous method consuming a large amount of time and computer memories, we developed the new controller which is more convenient to implement while keeps the same tracking accuracy.

This paper is organized as follows. Section II gives the dynamic model of the swing phase with joint friction torques. Section III presents the system identification experiments and its validation results. Section IV describes the proposed control method with stability analysis. Experimental results are shown in section V. In the end, discussions and future work are given in section VI.

II. DYNAMIC MODELLING

A. Swing Phase Model

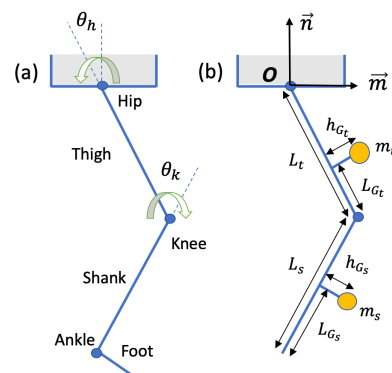


Fig. 1 Schematic diagram of swing phase.

During the swing phase, the swing leg is in the air and has no interaction with the environment. Since the motion of swing leg is constrained within the sagittal plane with the passive ankle joint, one 2D two-segment manipulator is established (Fig. 1a). The origin of the coordinates is set at the hip joint, and other symbols in Fig. 1b are defined as follows: θ_k and θ_h are the knee dorsiflexion and hip flexion, respectively; \vec{m} and \vec{n} are the unit vectors of two coordinate axes; m_t and m_s represent the mass of thigh segment and shank segment; L_t and L_s denote the length of thigh segment and shank segment; J_t and J_s are the inertia of thigh segment and shank segment; (L_{Gt}, h_{Gt}) and (L_{Gs}, h_{Gs}) are the coordinates of the centre of gravity (COG) of each segment with respect to the distal joint.

The coordinates of COG of thigh segment and shank segment are expressed by r_t and r_s , respectively. Besides, $\Delta\theta$ is defined as the angle differences between knee joint angle and hip joint angle ($\Delta\theta = \theta_k - \theta_h$).

$$\begin{aligned} r_t &= [(L_t - L_{Gt}) \sin \theta_h + h_{Gt} \cos \theta_h] \vec{m} \\ &+ [-(L_t - L_{Gt}) \cos \theta_h + h_{Gt} \sin \theta_h] \vec{n}. \end{aligned} \quad (1)$$

$$\begin{aligned} r_s &= [L_t \sin \theta_h - (L_s - L_{Gs}) \sin(\Delta\theta) \\ &+ h_{Gs} \cos(\Delta\theta)] \vec{m} \\ &+ [-L_t \cos \theta_h - (L_s - L_{Gs}) \cos(\Delta\theta) \\ &- h_{Gs} \sin(\Delta\theta)] \vec{n}. \end{aligned} \quad (2)$$

The thigh segment velocity v_t and shank segment velocity v_s are obtained by differentiating r_t and r_s with respect to time. Thus, the kinematic energy (T) and potential energy (V) with respect to the hip joint can be further expressed by (3) and (4), respectively, as follows:

$$T = \frac{1}{2} m_t v_t^2 + \frac{1}{2} J_t (\dot{\theta}_h)^2 + \frac{1}{2} m_s v_s^2 + \frac{1}{2} J_s (\dot{\theta}_k - \dot{\theta}_h)^2. \quad (3)$$

$$\begin{aligned} V &= -[(L_t - L_{Gt}) \cos \theta_h - h_{Gt} \sin \theta_h] m_t g \\ &- [L_t \cos \theta_h + (L_s - L_{Gs}) \cos(\Delta\theta) \\ &+ h_{Gs} \sin(\Delta\theta)] m_s g. \end{aligned} \quad (4)$$

As the swing leg has two external inputs, the torque of each joint (5) can be calculated by using Lagrangian mechanics ($i = h$, hip joint; $i = k$, knee joint).

$$A_i = \frac{d}{dt} \left(\frac{\partial(T - V)}{\partial \dot{\theta}_i} \right) - \frac{\partial(T - V)}{\partial \theta_i}, \quad (5)$$

where A_i denotes the input joint torque of the swing leg.

B. Joint Friction Torques

Under ideal conditions, the input torque at each joint is equal to the motor output torque. However, Ghan et al. [11] found that different types of friction torque also influence the torques exerted on the exoskeleton. Let τ_i denote the motor output torque. Then

$$\tau_i = A_i + B_i(\theta_i) + C_i(\dot{\theta}_i) \quad (6)$$

where $B_i(\theta_i)$ and $C_i(\dot{\theta}_i)$ represent stiffness friction torque and damping friction torque, respectively. Besides, we assume the stiffness friction torque $B_i(\theta_i)$ is a function of joint angle and the damping torque $C_i(\dot{\theta}_i)$ is only related to the joint

angular velocity. The total torque model of hip joint and knee joint can be written respectively, as follows.

$$\begin{aligned} \tau_h &= \{m_t[(L_t - L_{Gt})^2 + h_{Gt}^2] + J_t \\ &+ m_s[(L_s - L_{Gs})^2 + h_{Gs}^2] + J_s \\ &+ 2L_t[m_s(L_s - L_{Gs}) \cos \theta_k + m_s h_{Gs} \sin \theta_k]\} \ddot{\theta}_h \\ &- \{m_s[(L_s - L_{Gs})^2 + h_{Gs}^2] + J_s \\ &+ L_t[m_s(L_s - L_{Gs}) \cos \theta_k - m_s h_{Gs} \sin \theta_k]\} \ddot{\theta}_k \\ &+ L_t[m_s(L_s - L_{Gs}) \sin \theta_k] \dot{\theta}_k \\ &- m_s h_{Gs} \cos \theta_k](\dot{\theta}_k - 2\dot{\theta}_h) \dot{\theta}_k + [m_t(L_t \\ &- L_{Gt}) \sin \theta_h + m_t h_{Gt} \cos \theta_h] g + [m_s L_t \sin \theta_h \\ &- m_s(L_s - L_{Gs}) \sin(\Delta\theta) + m_s h_{Gs} \cos \Delta\theta] g \\ &+ B_h(\theta_h) + C_h(\dot{\theta}_h). \end{aligned} \quad (7)$$

$$\begin{aligned} \tau_k &= \{-m_s[(L_s - L_{Gs})^2 + h_{Gs}^2] - J_s \\ &- L_t[m_s(L_s - L_{Gs}) \cos \theta_k + m_s h_{Gs} \sin \theta_k]\} \ddot{\theta}_h \\ &+ \{m_s[(L_s - L_{Gs})^2 + h_{Gs}^2] + J_s\} \ddot{\theta}_k + L_t[m_s(L_s \\ &- L_{Gs}) \sin \theta_k - m_s h_{Gs} \cos \theta_k] \dot{\theta}_h \\ &+ [m_s(L_s - L_{Gs}) \sin(\Delta\theta) - m_s h_{Gs} \cos(\Delta\theta)] g \\ &+ B_k(\theta_k) + C_k(\dot{\theta}_k). \end{aligned} \quad (8)$$

C. Dynamic Model with Unknown Terms/Functions

While the joint angle and angular velocity of each joint can be measured directly, other parameters in (7) and (8) such as mass and inertia parameters, need to be determined by the system identification method. A minimal set of six parameters ($X_1, X_2, Y_1, Y_2, J_1, J_2$) is defined to describe all unknown constant parameters in (7) and (8), and the converted relationships are shown in Table I. Moreover, the dynamic model also contains some unknown functions, which are the stiffness friction torque $B_i(\theta_i)$ and the damping friction torque $C_i(\dot{\theta}_i)$. And they will be identified by experiments as well.

The overall dynamic model of the swing phase in vector form is as follows:

$$\begin{bmatrix} \tau_h \\ \tau_k \end{bmatrix} = M(\theta) \begin{bmatrix} \ddot{\theta}_h \\ \ddot{\theta}_k \end{bmatrix} + C(\theta, \dot{\theta}) \begin{bmatrix} \dot{\theta}_h \\ \dot{\theta}_k \end{bmatrix} + G(\theta) + F_r(\theta, \dot{\theta}), \quad (9)$$

where $M(\theta) \in R^{2 \times 2}$ represents the mass matrix of swing leg, $C(\theta, \dot{\theta}) \in R^{2 \times 2}$ represents the Coriolis and centripetal matrix, $G(\theta) \in R^2$ represents the gravity vector and $F_r(\theta, \dot{\theta}) \in R^2$ represents the friction torque vector.

TABLE I. MINIMAL SET OF UNKNOWN PARAMETERS

Parameters	Unknown Terms
Mass Moment	$X_1 = m_t(L_t - L_{Gt}) + m_s L_t$, $Y_1 = m_t h_{Gt}$, $X_2 = m_s(L_s - L_{Gs})$, $Y_2 = m_s h_{Gs}$
Inertia	$J_2 = m_s[(L_s - L_{Gs})^2 + h_{Gs}^2] + J_s$, $J_1 = m_t[(L_t - L_{Gt})^2 + h_{Gt}^2] + m_s L_t^2 + J_2$

In terms of the set of six parameters ($X_1, X_2, Y_1, Y_2, J_1, J_2$), various matrices and vectors in (9) are described as follows:

$$M(\theta) = \begin{bmatrix} M_{11}(\theta) & M_{12}(\theta) \\ M_{12}(\theta) & M_{22}(\theta) \end{bmatrix}. \quad (10)$$

$$C(\theta, \dot{\theta}) = \begin{bmatrix} C_{11}(\theta, \dot{\theta}) & C_{12}(\theta, \dot{\theta}) \\ C_{21}(\theta, \dot{\theta}) & 0 \end{bmatrix}. \quad (11)$$

$$G(\theta) = \begin{bmatrix} G_h(\theta) \\ G_k(\theta) \end{bmatrix}. \quad (12)$$

$$F_r(\theta, \dot{\theta}) = \begin{bmatrix} F_{rh}(\theta, \dot{\theta}) \\ F_{rk}(\theta, \dot{\theta}) \end{bmatrix}. \quad (13)$$

$$M_{11}(\theta) = 2L_t(X_2 \cos\theta_k + Y_2 \sin\theta_k) + J_1 + J_2. \quad (14)$$

$$M_{12}(\theta) = -L_t(X_2 \cos\theta_k + Y_2 \sin\theta_k) - J_2. \quad (15)$$

$$M_{22}(\theta) = J_2. \quad (16)$$

$$C_{11}(\theta, \dot{\theta}) = -L_t(X_2 \sin\theta_k - Y_2 \cos\theta_k) \cdot \dot{\theta}_k \quad (17)$$

$$C_{12}(\theta, \dot{\theta}) = L_t(X_2 \sin\theta_k - Y_2 \cos\theta_k) \cdot (\dot{\theta}_k - \dot{\theta}_h). \quad (18)$$

$$C_{21}(\theta, \dot{\theta}) = L_t(X_2 \sin\theta_k - Y_2 \cos\theta_k) \cdot \dot{\theta}_h. \quad (19)$$

$$G_h(\theta) = [X_1 \sin\theta_h + Y_1 \cos\theta_h - X_2 \sin(\Delta\theta) + Y_2 \cos(\Delta\theta)] \cdot g. \quad (20)$$

$$G_k(\theta) = [X_2 \sin(\Delta\theta) + \theta_k + Y_2 \cos(\Delta\theta)] \cdot g. \quad (21)$$

$$F_{rh}(\theta, \dot{\theta}) = B_h(\theta_h) + C_h(\dot{\theta}_h). \quad (22)$$

$$F_{rk}(\theta, \dot{\theta}) = B_k(\theta_k) + C_k(\dot{\theta}_k). \quad (23)$$

III. SYSTEM IDENTIFICATION

The principle of system identification is to control the swing leg to track desired reference trajectories, and then use the least squares method to find the relationship between joint torques and joint angles/angular velocities. Joint angles and angular velocities are measured by potentiometer and encoder, respectively. Motor torque is calculated by computing the product of motor current and motor torque constant. Besides, experimental data are processed by exponential moving average filter to reduce signal noise.

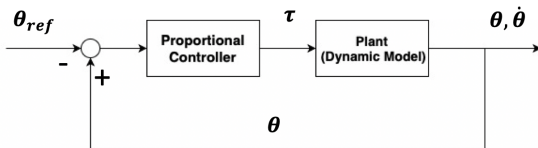


Fig. 2 Block diagram of system identification experiments.

The proportional controller $\tau = K[\theta - \theta_{ref}]$, where K is a positive control gain, is used as the control torque to the dynamic model of the swing leg (Fig. 2). According to different types of reference signal (θ_{ref}), identification experiments can be classified as static experiment and dynamic experiments. The reference signal for static experiments is a series of fixed point (step functions), and the measurements are taken when joint angular velocities are zero. For the dynamic part, hip and knee joints are regulated to track time varying

signals shown in Table II, and the joint sensor information is measured while the motor is rotating.

A. Experimental Procedure

The procedure of system identification experiments is summarized in Table II. Static experiments are taken twice to identify stiffness friction torque and mass moment parameters of hip joint and knee joint. On the other hand, inertia parameters and damping friction torques of hip joint and knee joint are estimated by dynamic experiments.

TABLE II. PROCEDURE OF SYSTEM IDENTIFICATION EXPERIMENTS

No.	Type	Identified terms	Reference trajectories
1	Static	Stiffness B_k, B_h	Start from 10 [deg] and choose knee reference every 5 [deg]. Select hip reference such that $\Delta\theta = \theta_k - \theta_h$ keeps the same value.
2	Static	Mass X_1, Y_1, X_2, Y_2	Randomly select 40 pairs of desired positions.
3	Dynamic	Inertia J_1, J_2	$\theta_{kref} = 20[\text{deg}], \theta_{href} = 40 + 20 \sin(0.1\pi t) [\text{deg}]$.
4	Dynamic	Damping C_k	$\theta_{kref} = 40 + 20 \sin(0.1\pi t) [\text{deg}], \theta_{href} = 20[\text{deg}]$.
5	Dynamic	Damping C_h	$\theta_{kref} = 20[\text{deg}], \theta_{href} = 40 + 20 \sin(0.1\pi t) [\text{deg}]$.

Due to page restrictions, more details regarding the system identification of the lower limb exoskeleton can be referred to the literature [11].

B. Model Validation

After processing experimental data, the results of system identification are listed in Table III. Another validation experiment is taken to verify the accuracy of the identified model. The hip joint and knee joint are controlled to track the same trajectory ($\theta_h = \theta_k = 40 + 20 \cdot \sin(0.4\pi t)$ [deg]), and the period of this test is one minute.

TABLE III. IDENTIFIED PARAMETERS AND FRICTION TORQUES

	Hip Joint	Knee Joint
Mass Moment Parameters [kgm]	$X_1 = 0.2567, Y_1 = -1.5967$	$X_2 = -0.6023, Y_2 = -0.6240$
Inertia Parameters [kgm ²]	$J_1 = 15.0022$	$J_2 = 3.1043$
Stiffness Friction Torque [Nm]	$B_h(\theta_h) = 0$	$B_k(\theta_k) = 0.039 \cdot \theta_k + b_{k0}$
Damping Friction Torque [Nm]	$C_h(\dot{\theta}_h) = -1.445 \cdot \text{sign}(\dot{\theta}_h) - 0.03776 \cdot \dot{\theta}_h - 16.39$	$C_k(\dot{\theta}_k) = -0.5929 \cdot \text{sign}(\dot{\theta}_k) - 0.1921 \cdot \dot{\theta}_k + 2.784$

The measured data are obtained directly from validation experiments, and the estimated torque-angle model is calculated by hip torque model (7), knee torque model (8) and the identified terms shown in Table III.

Comparing estimated torque model with measured torque data of validation experiments in Fig. 3, it is clear to see that the estimated model matches well with the measured torque.

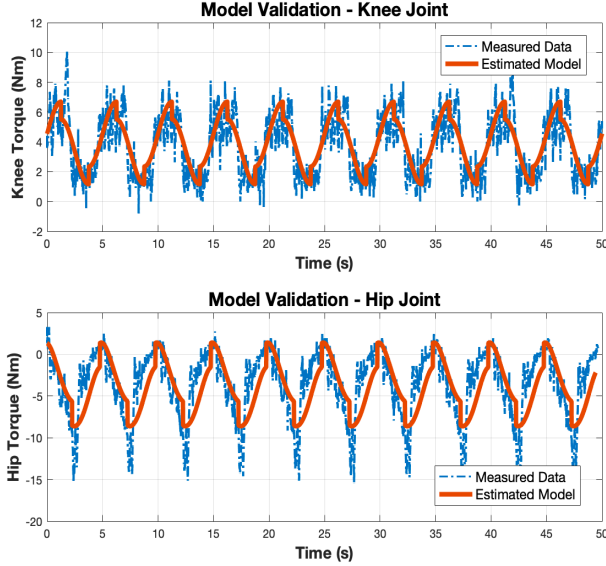


Fig. 3 Hip joint and knee joint validation experiment results.

C. Model Properties

The identified dynamic model of the swing phase has the following properties, which can be used to develop controller and analyze the stability of the closed-loop system.

Property 1: The inertia matrix $M(\theta)$ is symmetric and positive definite for all θ .

Property 2: The matrix $\frac{1}{2}\dot{M}(\theta) - C(\theta, \dot{\theta})$ is skew-symmetric for all θ and $\dot{\theta}$.

Proof: Define matrix $P(\theta, \dot{\theta}) \in R^{2 \times 2}$ to represent the matrix $\frac{1}{2}\dot{M}(\theta) - C(\theta, \dot{\theta})$.

$$P(\theta, \dot{\theta}) = \begin{bmatrix} \frac{1}{2}\dot{M}_{11}(\theta) - C_{11}(\theta, \dot{\theta}) & \frac{1}{2}\dot{M}_{12}(\theta) - C_{12}(\theta, \dot{\theta}) \\ \frac{1}{2}\dot{M}_{12}(\theta) - C_{21}(\theta, \dot{\theta}) & \frac{1}{2}\dot{M}_{22}(\theta) \end{bmatrix}$$

According to the equation (15), (18) and (19), it is clear to see that $\frac{1}{2}\dot{M}_{11}(\theta) - C_{11}(\theta, \dot{\theta})$ and $\frac{1}{2}\dot{M}_{22}(\theta)$ are equal to zero. Since

$$\begin{aligned} \frac{1}{2}\dot{M}_{12}(\theta) - C_{12}(\theta, \dot{\theta}) &= -[\frac{1}{2}\dot{M}_{12}(\theta) - C_{21}(\theta, \dot{\theta})] \\ &= L_t(X_2 \sin \theta_k - Y_2 \cos \theta_k) \left(\dot{\theta}_h - \frac{1}{2}\dot{\theta}_k \right), \end{aligned}$$

which implies $P(\theta, \dot{\theta}) = -P^T(\theta, \dot{\theta})$ and the matrix $P(\theta, \dot{\theta})$ is skew-symmetric.

Property 3: The Coriolis and centripetal matrix $C(\theta, \dot{\theta})$, gravity vector $G(\theta)$ and friction torque vector $F_r(\theta, \dot{\theta})$ in (9) are all bounded for all θ and $\dot{\theta}$.

IV. CONTROLLER DESIGN

The controller for the first prototype of the CUHK-EXO (Fig. 4) is divided into high level controller (PC) and lower level controller (MCU). Reference trajectories are computed and sent from high level controller to lower level controller by serial port communication, and the frequency is around 30Hz.

After receiving reference signals, the lower level controller will control DC motors to track desired trajectories by using the PD controller of the following form:

$$\tau = K_P(\theta_d - \theta) + K_D(\dot{\theta}_d - \dot{\theta}), \quad (24)$$

where $\theta \in R^2$ is the joint angle vector ($\theta = [\theta_h \ \theta_k]^T$), $\theta_d \in R^2$ is the vector of desired trajectories, and $K_P, K_D \in R^{2 \times 2}$ are positive definite matrices.

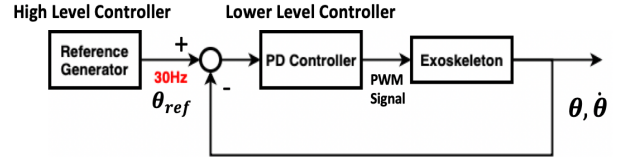


Fig. 4 Block diagram of pure PD controller.

By taking experiments with both healthy subject and paralyzed individual, we found this design has some limitations: 1) the transient response of the tracking error is quite large; 2) system communication frequency is low.

To improve the controller performance, we further consider the following nonlinear controller:

$$\tau = K_P(\theta_d - \theta) + K_D(\dot{\theta}_d - \dot{\theta}) + G(\theta) + F_r(\theta, \dot{\theta}). \quad (25)$$

We call this controller the PD controller with gravity and friction compensation. Under this control law, the block diagram in Fig. 4 is updated to Fig. 5. Moreover, the control frequency of the nonlinear controller is increased from 30 Hz to 100 Hz.

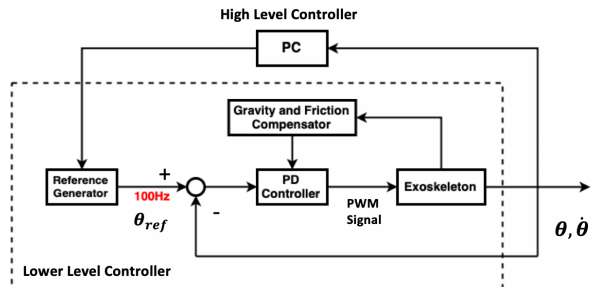


Fig. 5 Block diagram of nonlinear controller.

A. Desired Trajectory

The desired trajectories for walking are obtained from healthy walking subjects by the motion capture system, and each trajectory is a sum of sinusoidal functions (Fig. 6).

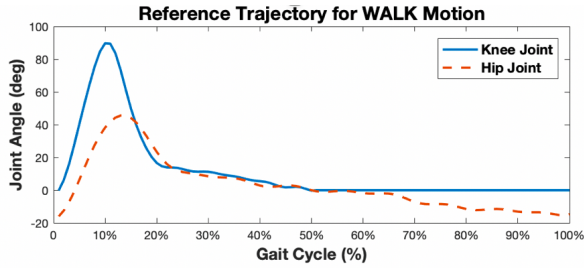


Fig. 6 Reference trajectory for ground walking.

The desired trajectories for walking are obtained from healthy walking subjects by the motion capture system, and each trajectory is a sum of sinusoidal functions (Fig. 6).

Since the exoskeleton has two active joints in one leg, the amplitudes of knee joint and hip joint trajectories are increased compared with normal gait references.

B. Stability Analysis

Let the tracking position error and velocity error be defined as $\tilde{\theta} \in \mathbb{R}^2$ ($\tilde{\theta} = \theta_d - \theta$) and $\dot{\tilde{\theta}} \in \mathbb{R}^2$ ($\dot{\tilde{\theta}} = \dot{\theta}_d - \dot{\theta}$), respectively. Substituting control law (25) into the torque equation of swing phase (9) gives the following closed-loop systems.

$$M(\theta)\ddot{\theta} + C(\theta, \dot{\theta})\dot{\theta} = K_p\tilde{\theta} + K_D\dot{\tilde{\theta}}. \quad (26)$$

In terms of the state vector $[\tilde{\theta}^T \quad \dot{\tilde{\theta}}^T]^T$, we can get

$$\frac{d}{dt}[\tilde{\theta}] = \begin{bmatrix} \dot{\tilde{\theta}} \\ \ddot{\theta}_d - M(\theta)^{-1}[K_p\tilde{\theta} + K_D\dot{\tilde{\theta}} - C(\theta, \dot{\theta})\dot{\theta}] \end{bmatrix}. \quad (27)$$

Assume θ_d is a constant, then the state vector becomes

$$\frac{d}{dt}[\tilde{\theta}] = \begin{bmatrix} -\dot{\theta} \\ M(\theta_d - \tilde{\theta})^{-1}[K_p\tilde{\theta} - K_D\dot{\tilde{\theta}} - C(\theta, \dot{\theta})\dot{\theta}] \end{bmatrix}. \quad (28)$$

In order to analyze the stability of the new developed controller, we use the following Lyapunov candidate function, which is proposed by Takegaki [12].

$$V(\tilde{\theta}, \dot{\theta}) = \frac{1}{2}\dot{\theta}^T M(\theta)\dot{\theta} + \frac{1}{2}\tilde{\theta}^T K_p\tilde{\theta}. \quad (29)$$

The time derivative of the Lyapunov candidate function is

$$\dot{V}(\tilde{\theta}, \dot{\theta}) = \dot{\theta}^T M(\theta)\ddot{\theta} + \frac{1}{2}\dot{\theta}^T \dot{M}(\theta)\dot{\theta} + \tilde{\theta}^T K_p\dot{\tilde{\theta}}. \quad (30)$$

Substituting the term $M(\theta)\ddot{\theta}$ from (28) into the derivative of the Lyapunov function gives

$$\begin{aligned} \dot{V}(\tilde{\theta}, \dot{\theta}) &= \dot{\theta}^T M(\theta)\ddot{\theta} + \frac{1}{2}\dot{\theta}^T \dot{M}(\theta)\dot{\theta} + \tilde{\theta}^T K_p\dot{\tilde{\theta}} \\ &= \dot{\theta}^T [K_p\tilde{\theta} - K_D\dot{\tilde{\theta}} - C(\theta, \dot{\theta})\dot{\theta}] + \frac{1}{2}\dot{\theta}^T \dot{M}(\theta)\dot{\theta} \\ &\quad - \tilde{\theta}^T K_p\dot{\tilde{\theta}} \\ &= \dot{\theta}^T \left[\frac{1}{2}\dot{M}(\theta) - C(\theta, \dot{\theta}) \right] \dot{\theta} - \dot{\theta}^T K_D\dot{\tilde{\theta}}. \end{aligned} \quad (31)$$

According to the Property 2, the matrix $\frac{1}{2}\dot{M}(\theta) - C(\theta, \dot{\theta})$ is skew-symmetric, which further implies

$$\dot{V}(\tilde{\theta}, \dot{\theta}) = -\dot{\theta}^T K_D\dot{\tilde{\theta}} \leq 0. \quad (32)$$

Since $\dot{V}(\tilde{\theta}, \dot{\theta})$ is negative semi-definite for all $\tilde{\theta}$ and $\dot{\theta}$, the function $V(\tilde{\theta}, \dot{\theta})$ is a Lyapunov function for (28). Thus, the state of the equilibrium point is stable.

To apply the La Salle's theorem to analyze the global asymptotic stability of the origin, let

$$\begin{aligned} \Omega &= \left\{ x = \begin{bmatrix} \tilde{\theta} \\ \dot{\theta} \end{bmatrix} \in \mathbb{R}^4 : \dot{V}(x) = 0 \right\} \\ &= \{ \tilde{\theta} \in \mathbb{R}^2, \dot{\theta} = 0 \in \mathbb{R}^2 \}. \end{aligned} \quad (33)$$

The trajectories of (28) that are contained in (33) are governed by the following equation

$$0 = M(\theta_d - \tilde{\theta})^{-1}(K_p\tilde{\theta}). \quad (34)$$

Since K_p is positive definite, equation (34) implies that the only trajectory of (28) contained in Ω is $[\tilde{\theta}^T \quad \dot{\theta}^T]^T = 0 \in \mathbb{R}^4$. Thus, according to the La Salle's Theorem [12], the equilibrium point $(\tilde{\theta}, \dot{\theta}) = (0, 0)$ is globally asymptotically stable.

V. EXPERIMENTAL RESULTS

In this section, the tracking performance of the new design controller is verified by experiments.

The hip joint of the exoskeleton is suspended on a fixed frame, and the swing leg has no interaction with the environment (Fig. 7). Besides, some sandbags are mounted on the thigh segment and shank segment as pay loads. The mass and inertia parameters of sandbags are calculated according to the anthropometry data from literature [14].

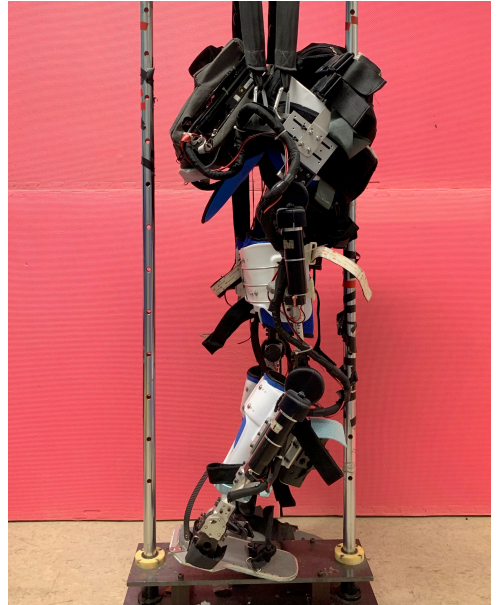


Fig. 7 Experimental setup of the CUHK-EXO.

With the gait period set at 10 seconds, the performance of the PD controller and PD controller with gravity and friction compensation (PDGC) are evaluated in terms of the capability of having the swing leg to track the reference signals.

It can be seen that the tracking errors under two control methods are all bounded as shown in Fig. 8. However, the

peak tracking errors of PDGC (hip joint: 10 [deg], knee joint: 5 [deg]) are significantly smaller than the peak tracking errors of PD controller (hip joint: 15 [deg], knee joint: 12 [deg]).

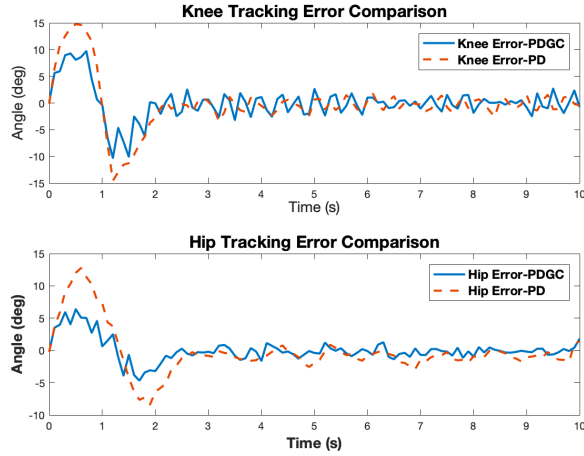


Fig. 8 Tracking error comparison of PD and PDGC.

Fig. 9 further compares the profiles of knee torque and hip torque of the two controllers. It can be seen that the control powers of the two controllers are comparable, which means the PDGC controller can improve the tracking performance while keeping about the same level of energy consumption as the PD controller.

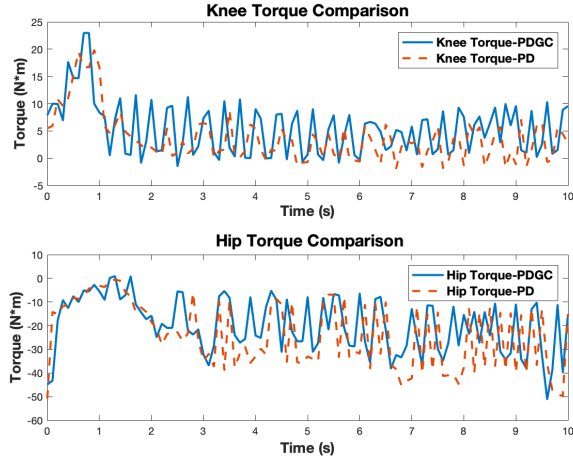


Fig. 9 Input torque comparison of PD and PDGC.

VI. CONCLUSION AND FUTURE WORK

In this paper, we have first established the dynamic model of the swing phase of the CUHK-EXO. Then we have conducted system identification experiments and verified the estimated model.

Based on the identified dynamic model, we have two controllers, namely, the PD controller and the PD controller with gravity and friction compensation. The latter controller can enhance the tracking performance of the swing phase during the swing phase.

For the future work, we will focus on the study of stance control problem and the coordination of different functions for the exoskeleton.

ACKNOWLEDGMENT

This work was supported by Research Grants Council (Project No. CUHK 14210019) of the Hong Kong Special Administrative Region, China, and Vice Chancellors Discretionary Fund/CUHK T Stone Robotics Institute (Project ID: 4930762).

REFERENCES

- [1] B. Chen, H. Ma, L.Y. Qin, F. Gao, K.M. Chan, S.W. Law, L. Qin and W.H. Liao, "Recent developments and challenges of lower extremity exoskeletons," *Journal of Orthopaedic Translation*, vol. 5, 2016, pp. 26-37.
- [2] S. Jezernik, G. Colombo, T. Keller, H. Frueh and M. Morari, "Robotic orthosis Lokomat: A rehabilitation and research tool," *Neuromodulation: Technology at the Neural Interface*, vol. 6, issue 2, 2003, pp. 108-115.
- [3] S. K. Banala, S. K. Agrawal and J. P. Scholz, "Active leg exoskeleton (ALEX) for gait rehabilitation of motor-impaired patients," *2007 IEEE 10th International Conference on Rehabilitation Robotics*, Noordwijk, 2007, pp. 401-407.
- [4] M. Talaty, A. Esquenazi and J. E. Briceño, "Differentiating ability in users of the ReWalk™ powered exoskeleton: An analysis of walking kinematics," *2013 IEEE 13th International Conference on Rehabilitation Robotics (ICORR)*, Seattle, WA, 2013, pp. 1-5.
- [5] R. J. Farris, H. A. Quintero, S. A. Murray, K. H. Ha, C. Hartigan and M. Goldfarb, "A preliminary assessment of legged mobility provided by a lower limb exoskeleton for persons with paraplegia," *IEEE Transactions on Neural Systems and Rehabilitation Engineering*, vol. 22, no. 3, May. 2014, pp. 482-490.
- [6] A. B. Zoss, H. Kazerooni and A. Chu, "Biomechanical design of the Berkeley lower extremity exoskeleton (BLEEX)," *IEEE/ASME Transactions on Mechatronics*, vol. 11, no. 2, Apr. 2006, pp. 128-138.
- [7] T. Kawabata, H. Satoh and Y. Sankai, "Working posture control of Robot Suit HAL for reducing structural stress," *2009 IEEE International Conference on Robotics and Biomimetics (ROBIO)*, Guilin, 2009, pp. 2013-2018.
- [8] B. Chen, C. H. Zhong, X. Zhao, H. Ma, X. Guan, X. Li, F. Y. Liang, C. Y. J. Cheng, L. Qin, S. W. Law, and W. H. Liao, "A wearable exoskeleton suit for motion assistance of paralyzed patients," *Journal of Orthopaedic Translation*, vol. 11, 2017, pp. 7-18.
- [9] B. Chen, C.H. Zhong, H. Ma, X. Guan, L.Y. Qin, K.M. Chan, S.W. Law, L. Qin, and W.H. Liao, "Sit-to-stand and stand-to-sit assistance for paraplegic patients with CUHK-EXO exoskeleton," *Robotica*, vol. 36, no. 4, 2018, pp. 535-551.
- [10] D.L. Castro, C.H. Zhong, F. Braghin, and W.H. Liao, "Lower limb exoskeleton control via linear quadratic regulator and disturbance observer," *2018 IEEE International Conference on Robotics and Biomimetics (ROBIO)*, Kuala Lumpur, 2018, pp. 1743-1748.
- [11] J. Ghan and H. Kazerooni, "System identification for the Berkeley lower extremity exoskeleton (BLEEX)," *Proceedings 2006 IEEE International Conference on Robotics and Automation, 2006. ICRA 2006*, Orlando, FL, 2006, pp. 3477-3484.
- [12] M. Takegaki and S. Arimoto, "A new feedback method for dynamic control of manipulators," *ASME J. Dyn. Sys., Meas., Control*, vol. 103, issue 2, Jun. 1981, pp. 119-125.
- [13] J. -J. E. Slotine and W. Li, *Applied Nonlinear Control*. Englewood Cliffs (N.J.): Prentice Hall, 1991, ch. 3.
- [14] D. A. Winter, *Biomechanics and Motor Control of Human Movement* (4th ed.). New York: Wiley, 2009, ch. 4.